*Nano Research* 2015, 8(7): 2251–2260
DOI 10.1007/s12274-015-0736-8
**Research Article**
ISSN 1998-0124
CN 11-5974/O4

# Three-dimensional multimodal sub-diffraction imaging with spinning-disk confocal microscopy using blinking/fluctuating probes

Xuanze Chen[§], Zhiping Zeng[§], Hening Wang, and Peng Xi (✉)

*Department of Biomedical Engineering, College of Engineering, Peking University, Beijing 100871, China*
[§] *These authors contributed equally to this work.*

**Received:** 3 September 2014
**Revised:** 19 October 2014
**Accepted:** 28 January 2015



**KEYWORDS**
multi-modality,
super-resolution microscopy,
three-dimensional,
spinning-disk confocal

## ABSTRACT

Three-dimensional imaging cannot be achieved easily using previously developed localization super-resolution techniques. Here, we present a three-dimensional multimodal sub-diffraction imaging technique with spinning-disk (SD) confocal microscopy called 3D-MUSIC, which not only has all the advantages of SD confocal microscopy, such as fast imaging speed, high signal-to-noise ratio, and optical-sectioning capability, but also extends its spatial resolution limit along all three dimensions. Both axial and lateral resolution can be improved simultaneously by virtue of the blinking/fluctuating nature of modified fluorescent probes, exemplified with the quantum dots. Further, super-resolution images with dual modality can be obtained through super-resolution optical fluctuation imaging (SOFI) and bleaching/blinking-assisted localization microscopy (BaLM). Therefore, fast super-resolution imaging can be achieved with SD-SOFI by capturing only 100 frames while SD-BaLM yields high-resolution imaging.

## 1 Introduction

Optical fluorescence microscopy has been routinely applied to investigate a vast variety of biological phenomena in the life sciences [1]. Confocal laser scanning microscopy (CLSM) is one of the most powerful and versatile diagnostic tools in the biomedical sciences, especially cell biology, owing to its unique ability to eliminate out-of-focus noise and excellent three-dimensional (3D) optical-sectioning capability [2–4]. In contrast to the conventional scanning mode, spinning-disk (SD) confocal microscopy uses an array of spirally arranged pinholes to form parallel scans across the specimen [5]. SD confocal microscopy enables the utilization of a charge-coupled device (CCD) detector to collect the confocal optical sectioning image from the specimen [6]. However, owing to wave nature of light, the spatial resolution of CLSM is limited to $1/\sqrt{2}$ times the Rayleigh diffraction limit, which is determined by the laser wavelength and numeral aperture (NA) [7–10]. Thus, to investigate intracellular objects, conventional CLSM or SD has met significant

Address correspondence to xipeng@pku.edu.cn

challenges in discerning fine structures beyond the diffraction limit. Consequently, a microscopic technique that can break the diffraction barrier is highly desirable for further biological research [11–13].

In the past decade, various super-resolution techniques aiming at breaking the diffraction barrier have been proposed [14–18], such as stimulated emission depletion microscopy (STED) [19, 20], saturated structured illumination microscopy (SSIM) [21, 22], photoactivated localization microscopy (PALM) [23, 24], stochastic optical reconstruction microscopy (STORM) [25, 26], bleaching/blinking-assisted localization microscopy (BaLM) [27], and super-resolution optical fluctuation imaging (SOFI) [28, 29]. It should be noted that as PALM and STORM are based on the localization of a wide-field image, 3D super-resolution imaging has to be implemented with sophisticated point spread function (PSF) modulation following data postprocessing, such as astigmatism [26] and double helix [30].

Among these super-resolution techniques [31], BaLM and SOFI are two novel super-resolution microscopy techniques that have the advantage of blinking/fluctuating probes to achieve contrast-enhanced super-resolution imaging. However, they differ in their algorithms: BaLM first uses subsequent subtraction for the captured adjacent image frames and then resolves the localization information using the single-particle localization method; SOFI extracts localization information from the temporal correlation statistics of pixel-intensity fluctuations, and the spatial resolution can be enhanced $n$-fold by calculating the $n^{\text{th}}$-order cross cumulant [32].

To obtain better performance of these blinking/localization-based super-resolution techniques, original images must be obtained with both a high imaging rate and high signal-to-noise ratio (SNR) for ensuring the correctness of super-resolution analysis algorithms. The commonly used probes, such as quantum dots (QDs) [33, 34], dyes [35], and photoswitchable fluorescent proteins [36–38], possess photoswitchability or the ability to blink/fluctuate. In particular, QDs have been widely used as an alternative fluorescent inorganic dye in both cellular and tissue imaging owing to their high brightness and photostability [39, 40]. Initially, blinking/fluctuation was treated as a negative effect and was suppressed through surface modification with special reagents. Later, it was utilized as a means for super-resolution imaging [41].

In this paper, we first realized three-dimensional multimodal sub-diffraction imaging based on SD confocal microscopy using QD fluctuating probes. QDs used in multimodal sub-diffraction imaging with SD confocal microscopy enables higher SNR and better 3D optical-sectioning ability, which results in 3D-multimodal sub-diffraction imaging with spinning-disk confocal (3D-MUSIC) microscopy. This multimodal sub-diffraction imaging technique allows features at any $z$ depth of the cell to be resolved.

## 2 Materials and methods

3D-MUSIC can easily achieve three-dimensional super-resolution imaging of subcellular structures labeled with blinking/fluctuating probes across a large field of view that simultaneously possesses good $z$-optical-sectioning capability.

The images of the microtubule networks were collected using an SD confocal fluorescence microscope (PerkinElmer UltraView VoX) with an oil objective (Nikon, 100x, NA 1.4). A laser of wavelength 405 nm was employed for exciting the fluorescence emission of QD625 (power density: 200 W/cm$^2$). The fluorescence signals were collected using an electron-multiplying CCD (EMCCD; Hamamatsu, C9100-13). The exposure time of each frame was 30 ms, and 1,000 frames were captured for each slice (200 nm along the $z$-axis for each slice). In the experiment, drift correction was realized without any fiducial beads. After the acquisition of time-lapse images, we implemented drift correction with sub-pixel precision based on discrete Fourier transforms and nonlinear optimization [42].

The spatio-temporal cross cumulants between neighboring pixels are calculated in the SOFI processing [32, 43]. An approximation of the underlying PSF can be well estimated by calculating the cross cumulants. Moreover, the spatial resolution can be linearly enhanced over the cumulant order by using Fourier reweighting. Additionally, the nonlinear response to brightness and blinking heterogeneities in SOFI processing can be prominently eliminated by analyzing

the blinking kinetics of the fluorophores using balanced SOFI (bSOFI). In this work, SOFI processing is performed with the bSOFI software using 100 images [32]. BaLM [27] was implemented using a custom Matlab program based on the subtraction of 1,000 images. Image subtraction was performed by subtracting consecutive images from the acquired image series: $J_i = I_n - I_{n-1}$, where $I_n$ and $I_{n-1}$ represent the captured image frames and $J_i$ represents the subtracted image slice. After subtraction, $J_i$ values were combined as an image stack for localization. Finally, single-molecule localization was performed on the subtracted image sequences using QuickPALM (ImageJ) [44].

## 3 Results

### 3.1 Schematic illustration

In Fig. 1, assuming a test sample labeled with blinking/fluctuating fluorophores, when applying illumination, the fluorophores intermittently emit fluorescence over the exposure time. This type of fluorescence intermittency (blinking/fluctuation) can be analyzed using the SOFI algorithm to improve the spatial resolution of the captured images. Furthermore, the captured image frames can be sequentially subtracted pairwise, isolating some sparsely distributed blinking events for localization-based super-resolution imaging. Finally, after localizing the individual fluorophores from the subtracted frames, a super-resolution image can be reconstructed using BaLM.

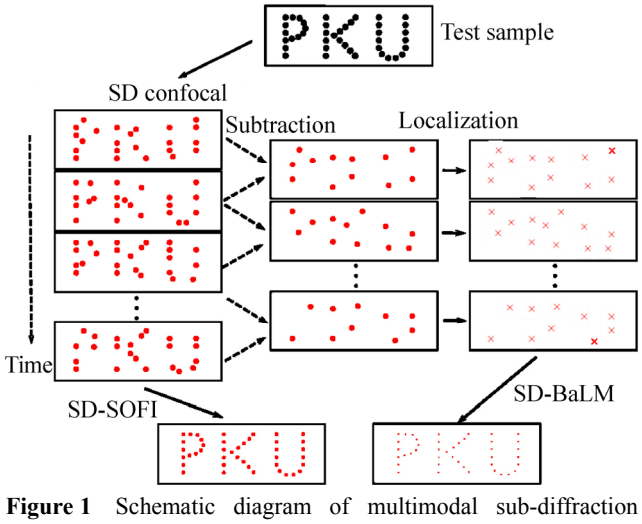


**Figure 1** Schematic diagram of multimodal sub-diffraction imaging with spinning-disk confocal microscopy using fluctuating probes.

### 3.2 Numerical simulations

The labeling density is of great importance for reflecting the structure faithfully in biological fluorescence imaging, especially for super-resolution microscopy [45]. In this simulation, we chose three letters written as "PKU" as the test object and simulated the blinking process of the fluorophores distributed on the test object under various labeling densities ranging from 5 to 24 μm$^{-1}$, as shown in Fig. 2. Here, the pixel number in the simulation was set to 240 × 240 with a pixel size of 20 nm. The simulated PSF was calculated based on the emission wavelength of the QDs and the numerical aperture of the objective. In general, the FWHM of the PSF is given by the Abbe diffraction equation

$$d \approx \frac{0.51\lambda}{\mathrm{NA}}$$

in which $\lambda$ is the wavelength of the excitation, and NA is the numerical aperture of the microscopy objective.

The peak emission wavelength of QD625 used in our experiment is 625 nm, with an objective of NA 1.4. Therefore, the FWHM of the PSF is approximately 228 nm. The blinking process was simulated by generating 1,000 frames of blinking fluorophores on the test object. The blinking of each point follows a rate ratio $r$ of 5, i.e.

$$r = \frac{t_{\mathrm{off}}}{t_{\mathrm{on}}}$$

which implies that the blinking off time $t_{\mathrm{off}}$ is statistically 5 times the blinking on time $t_{\mathrm{on}}$. After simulation, the averaged, SD-SOFI, and SD-BaLM images were reconstructed using bSOFI and custom-written BaLM algorithms (Matlab, MathWorks). When the labeling density is low (i.e., < 7 μm$^{-1}$), the complete structure of the test image cannot be reconstructed after SD-SOFI and SD-BaLM processing. SD-SOFI generated results with severe discontinuities. In particular, SD-BaLM totally fails to present structurally observable results. When increasing the labeling densities, the integrity of the test image can be well maintained in both SD-SOFI and SD-BaLM processing. However, if the labeling densities are excessively high (typically >14 μm$^{-1}$), high-order SD-SOFI processing has undesirably induced artifacts.

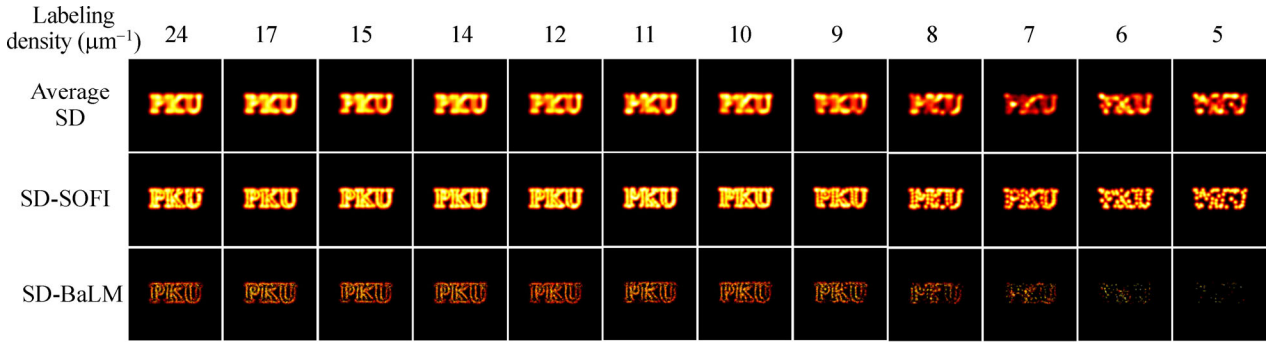


**Figure 2** Numerical simulations of average, SD-SOFI (3rd cumulant), and SD-BaLM images under different labeling densities.

Unlike PALM/STORM techniques, which typically discard data from molecules with overlapping images, dominant overlapping events are allowed in our simulation. As can be seen, the test object was blurred in the averaged image displayed in Fig. 2, which is due to the insufficient spatial resolution in SD confocal microscopy. In contrast, by applying SD-SOFI processing, the detailed structures of the test object can be clearly discerned, demonstrating that SD-SOFI has the capability of reconstructing sub-diffraction images even when the overlapping events are dominant. Subsequently, SD-BaLM was introduced for achieving single-molecule localization microscopy based on image subtraction. We generated 2,000 frames for blinking-assisted localization. After localization and image reconstruction, the resolution can be further improved compared to both those of the average SD and SD-SOFI counterparts. Correlation coefficients of the target image with the average, SD-SOFI, and SD-BaLM are shown in Fig. S1 (in the Electronic Supplementary Material (ESM)).

To test the noise resistance and robustness of the proposed multimodal method, a random noise was taken into consideration in Fig. S2 (in the ESM).

### 3.3 Super-resolution imaging based on spinning-disk confocal microscopy

The microtubules in COS7 cells were labeled using QD625 with a labeling density of 17 $\mu m^{-1}$ in our experiment. A laser of wavelength 405 nm was applied for fluorescence excitation. An SD confocal microscope was utilized for super-resolution imaging, which was achieved through the blinking/fluctuation behavior of QDs. During the experiment, one thousand conventional SD confocal images were collected for reconstructing a super-resolution image. In Fig. 3(a), the collected one thousand images were superimposed, generating an average image of the microtubule networks. After 2nd- or 3rd-order SOFI processing, the background noise was well suppressed, and the SNR had been significantly improved. The intensity plot in Fig. 3(e) indicates that the FWHMs for SD confocal microscopy and 3rd-order SD-SOFI are 390 and 180 nm, respectively. Here, the central wavelength of fluorescence emission is 625 nm, and an objective with NA = 1.4 is employed; therefore, the theoretical resolution is ~228 nm. For SD microscopy, the resolution is generally poorer than the theoretical prediction because the objective aperture is not filled and the confocal pinhole is relatively large. Owing to the localization process, SD-BaLM can improve the resolution to 40 nm in our experiment. The intensity fluctuation of a single pixel in SD microscopy is presented in Fig. 3(f), and its Poisson blinking-intensity statistics distribution shown in Fig. 3(g) indicates that QDs do not suffer from the higher-order analysis [46].

### 3.4 Three-dimensional super-resolution imaging based on spinning-disk confocal microscope

The axial resolution $r_z$ of conventional far-field microscopy is always limited by the diffraction to by greater than 600 nm, which can be mathematically described by the following equation [47]

$$r_z = \frac{2n\lambda}{\mathrm{NA}^2}$$

where $\lambda$ is the wavelength of the excitation, $n$ is the refractive index of the immersion medium, and

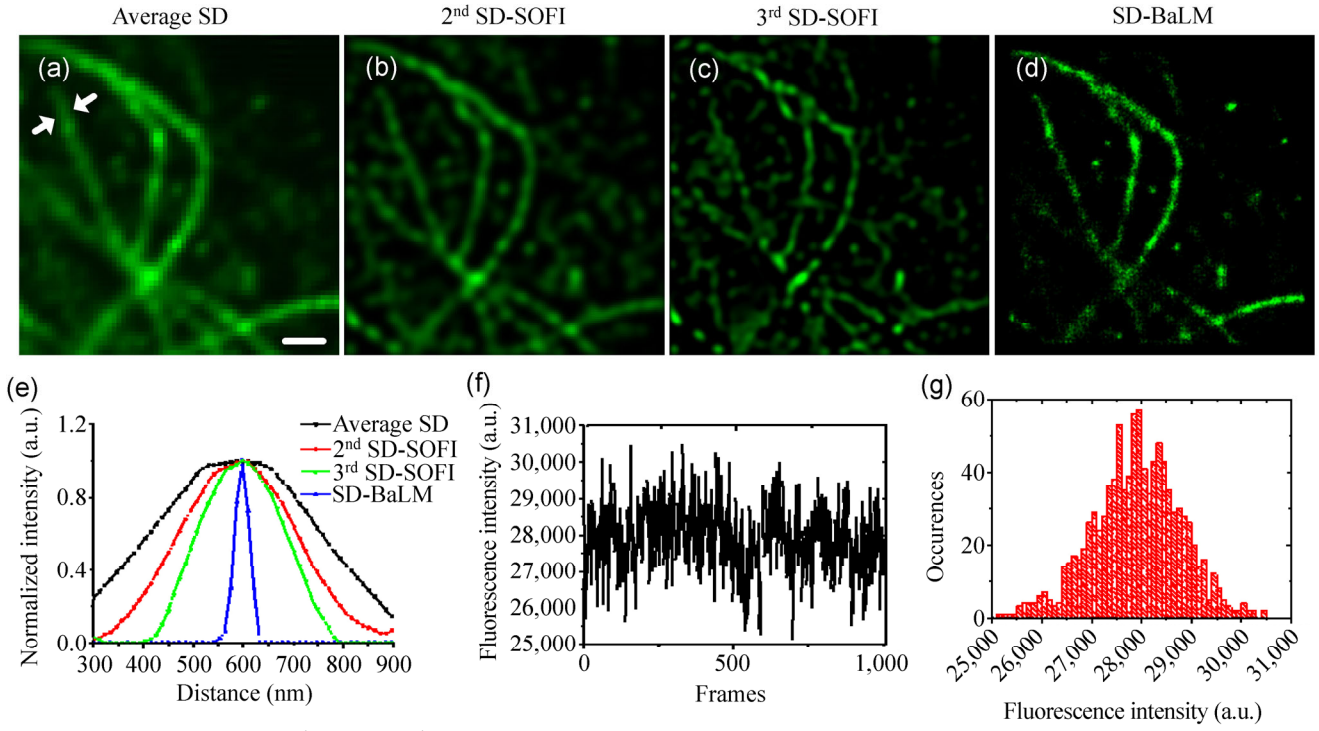


**Figure 3** (a) Average, (b) 2nd, and (c) 3rd SOFI super-resolution imaging of 100 frames based on spinning-disk confocal microscope (SD); (d) SD-BaLM based on the 2,000 frames subtracted from the 1,000 original image data. (e) Intensity profile of cross sections along the white arrow, as indicated in the upper panels. (f) Intensity fluctuation of a single pixel in SD microscopy. (g) Histogram distribution of (f). Scale bar: 1 μm.

NA is the numerical aperture of the objective. For confocal microscopy, as the focused excitation laser is coupled with pinhole-restricted detection, the axial resolution can be improved, in principle, by up to a factor of 1.4 [47].

Straightforward 3D super-resolution imaging of SOFI was demonstrated using a wide-field (WF), lamp-based optical microscope [46]; however, the SNR of WF microscopy is much worse than that of SD confocal microscopy because of the lack of optical sectioning capability in WF microscopy. Figure 4 shows that the SNR in SD microscopy can be improved by a factor of approximately 5 compared to the SNR in WF microscopy (the detailed method is shown in Fig. S3 in the ESM).

To determine the enhancement in axial resolution, $x$–$z$ cross sections of different-order SD-SOFI 3D stacks are presented in Figs. 5(a)–5(d), and intensity profiles along the $z$ direction are plotted in Fig. 5(e). For each slice, 100 frames (200 nm along the $z$-axis for each slice) were captured for 3D SD-SOFI reconstruction, and the exposure time for each frame was 30 ms. As

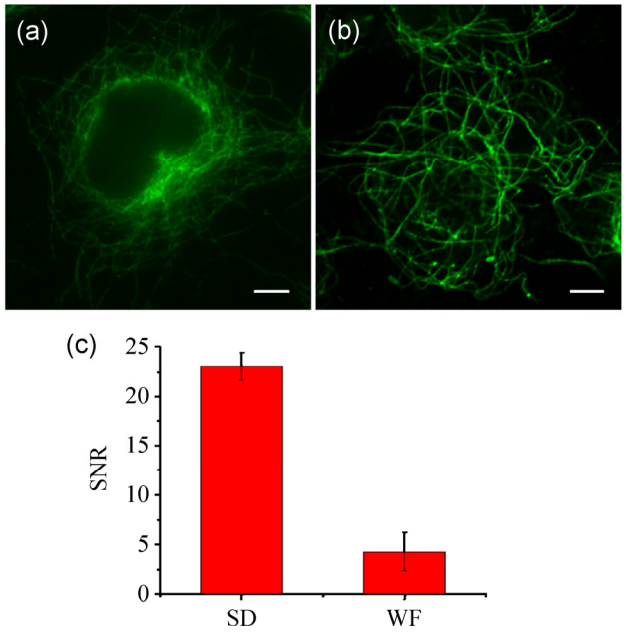


**Figure 4** Quantitative analysis and comparison of SNR between (a) WF microscopy and (b) SD confocal microscopy; (c) SNR comparison between SD and WF images. Scale bar: (a) 10 and (b) 5 μm.

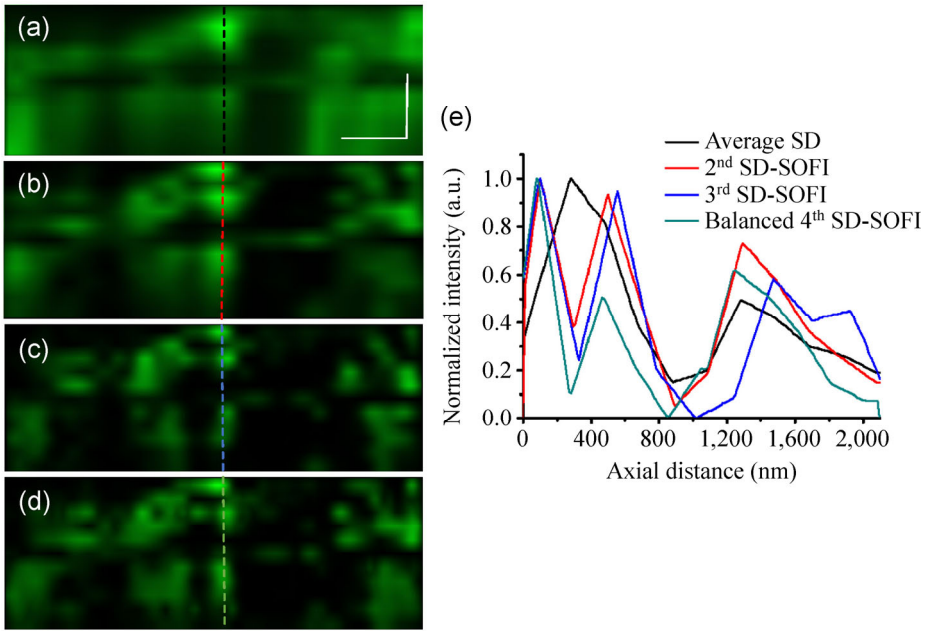


**Figure 5** (a) Average SD, (b) 2nd SD-SOFI, (c) 3rd SD-SOFI, and (d) balanced 4th SD-SOFI super-resolution imaging of 100 frames based on SD confocal microscopy of $x$–$z$ sections. (e) Vertical ($x$–$z$) cross sections of the three-dimensional dataset plotted on dashed lines of (a)–(d). Scale bar: 1 μm.

shown in Fig. 5(e), 450-nm $z$-resolution of SD confocal microscopy is well fitted with the relationship between SD and WF; better $z$-resolution was achieved when a higher-order SD-SOFI cumulant was used, which demonstrates the inherent super-resolution sectioning capability of SD-SOFI.

## 4 Discussion

Figure 6 shows a schematic diagram of PSFs in various microscopy modalities. WF fluorescence microscopy usually suffers from out-of-focus blur, which worsens both the lateral and axial resolutions. Although the total internal reflection fluorescence (TIRF) microscope possesses good SNR, this type of imaging system is not suitable for all biological investigations because of its limited imaging depth. In addition, TIRF lacks three-dimensional imaging capability. In SD confocal microscopy, multiple pinholes are introduced for fast imaging. The introduction of pinholes also enhances the lateral resolution and optical-sectioning capability along the axial direction. However, the resolution is still limited by the diffraction. By applying SD-SOFI processing, the PSF size can be significantly reduced in all three dimensions. Moreover, higher-order SD-SOFI processing generates a smaller PSF, which is far below the diffraction-limited size. In SD-BaLM processing, the localization precision could be decreased to the nanometer scale, achieving a resolution of less than 30 nm. The axial resolution, however, is also constrained by the PSF of the SD confocal system [15, 48].

Optical sectioning can be performed using confocal microscopy. In comparison to conventional confocal microscopy, SD confocal microscopy is more suitable for SOFI. In SD confocal microscopy, assuming that there are $N$ pixels on the CCD detector and that the number of SD spots at the detector is $M$, the effective dwell time for each pixel can be expressed as $(M/N) \times T$, where $T$ is the frame time. In comparison, the pixel dwell time for WF microscopy is $t_{WF} = T$, whereas the pixel dwell time for a conventional confocal point scanning microscope is $t_{confocal} = T/N$. As the calculation of the cross cumulants in SOFI rely on a relatively long pixel dwell time $t$ and short frame time $T$, we can define the temporal aspect ratio as

$$A = t/T$$

Therefore, the temporal aspect ratio of SD confocal microscopy ($A = M/N$) is comparable to that of WF

| | Wide-field ($\lambda$ = 625 nm, $n$ = 1.52, NA = 1.4) | TIRF | Spinning-disk confocal | $n^{th}$ order SD-SOFI | SD-BaLM |
|---|---|---|---|---|---|
| $PSF_{xy}$ (nm) | 228 | 228 | $1-\sqrt{2}$ fold | $n-\sqrt{2}\,n$ fold | 30 |
| $PSF_z$ (nm) | >970 | ~100 | $1-\sqrt{2}$ fold | $n-\sqrt{2}\,n$ fold | $1-\sqrt{2}$ fold |

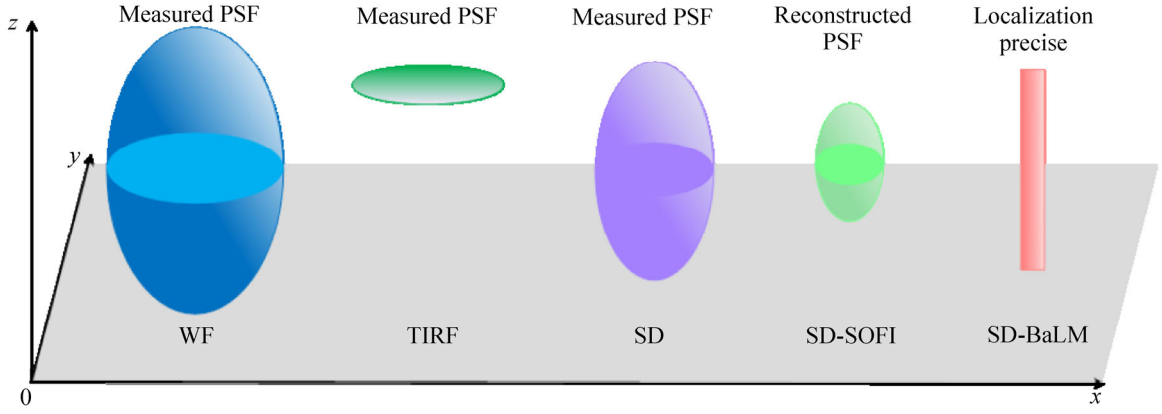


**Figure 6** Illustration of resolution scaling for different methods. As can be seen, SD confocal microscopy can provide up to 1.4-fold resolution enhancement depending on the pinhole size, in addition to optical sectioning. The $n^{th}$-order SOFI can provide $n$-fold resolution scaling. Therefore, SD-SOFI can provide $\sqrt{2}\,n$-fold resolution enhancement compared to the diffraction-limited WF microscopy, in both lateral and axial resolutions. Although SD-BaLM can provide precise localization, its axial resolution is limited by the SD confocal microscope.

microscopy ($A$ = 1) for SOFI, which is much larger than that of point-scanning confocal microscopy ($A$ = $1/N$). Further, the short frame time in SD confocal microscopy makes it very attractive for SD-BaLM.

However, the major limitation to 3D-SOFI is that it relies on the blinking/fluctuation of the fluorescent labels. QDs are the most popular type of fluorophore for SOFI, but other blinking fluorescent proteins have been used in SOFI [49]. Furthermore, the resolution scaling for SOFI is linearly proportional to the high-order SOFI process, which can induce artifacts. In this work, we used 100 frames for each layer of SD-SOFI reconstruction, which takes 3 s. With the blinking-enhanced QD, the temporal resolution could be improved by 10 times or with only 10 frames [50].

For 3D-BaLM, the bleaching/blinking ratio must be controlled to be less than 1 bleaching/blinking molecule per unit PSF area during each pixel dwell time to guarantee the localization precision. Two parameters are involved: the bleaching/blinking ratio (temporal criterion) and the labeling density (spatial criterion). An excessive bleaching/blinking ratio can cause an error (overlapped emission within one pixel dwell time) in the localization in BaLM, while a low bleaching/blinking ratio requires more frames for reconstruction.

Meanwhile, a relatively low labeling density can ease both SOFI and BaLM from possible overlapping molecules within one PSF area to generate reconstruction artifact. However, a high labeling density ensures the fidelity of the final image to reflect the subcellular structure. Recently, we introduced joint-tagging SOFI, in which QDs are used with different spectra, to circumvent this problem through simultaneous multi-spectral channel detection. In each channel, the labeling density is relatively low, whereas the summed labeling density of multiple channels is sufficiently high to reflect the structure in detail [51].

## 5 Conclusions

Previous super-resolution techniques require a complicated setup to achieve three-dimensional super-resolution, which limits their applicability. We proposed a 3D-MUSIC using fluctuation probes, which takes advantage of the 3D optical sectioning capability of spinning-disk confocal microscopy and makes use of the intrinsic fluctuation behavior of fluorescent probes.

Although the spatial resolution of 3D-MUSIC may be an inherent weakness in comparing with other single-molecule localization-based super-resolution techniques, the advantages of 3D-MUSIC could be summarized as follows: (1) Its time resolution is much better than in conventional localization super-resolution techniques; (2) it is simple and practical because it does not require engineered photon-switchable or photo-activated fluorescent proteins, although these fluorescent probes should also work; (3) it shows excellent signal-to-noise ratios and 3D optical-sectioning ability using spinning-disk confocal microscopy; (4) it allows better intracellular super-resolution compared with TIRF or WF microscopy. It is expected that combining 3D-MUSIC with compressed sensing would improve both the time and spatial resolution to achieve super-resolution images *in vivo* because of its excellent 3D optical-sectioning ability and better temporal resolution [52]. Further, it should be noted that the fluorescent label in 3D-MUSIC is not restricted to QDs; other blinking/fluctuating dyes such as photo-switchable fluorescent proteins [41], carbon nanodots [53, 54], and nitrogen-vacancy centers in fluorescent nanodiamond [55], are also suitable as fluorescent labels for this method.

## Acknowledgements

This work was supported by the National Instrumentation Program (No. 2013YQ03065102), the National Basic Research Program of China (Nos. 2011CB809101 and 2010CB933901), and the National Natural Science Foundation of China (Nos. 61178076, 31327901 and 61475010).

**Electronic Supplementary Material**: Supplementary material (cell preparation, comparisons of simulation results with noise, SNR calculation of Fig. 4) is available in the online version of this article at http://dx.doi.org/10.1007/s12274-015-0737-7.

## References

[1] Giloh, H.; Sedat, J. W. Fluorescence microscopy: Reduced photobleaching of rhodamine and fluorescein protein conjugates by n-propyl gallate. *Science* **1982**, *217*, 1252–1255.

[2] Baschong, W.; Suetterlin, R.; Laeng, R. H. Control of autofluorescence of archival formaldehyde-fixed, paraffin-embedded tissue in confocal laser scanning microscopy (CLSM). *J. Histochem. Cytochem.* **2001**, *49*, 1565–1571.

[3] Carlsson, K.; Danielsson, P. E.; Liljeborg, A.; Majlöf, L.; Lenz, R.; Åslund, N. Three-dimensional microscopy using a confocal laser scanning microscope. *Opt. Lett.* **1985**, *10*, 53–55.

[4] Wang, Y.; Kuang, C.; Cai, H.; Li, S.; Liu, W.; Hao, X.; Ge, J.; Liu, X. Sub-diffraction imaging with confocal fluorescence microscopy by stochastic photobleaching. *Opt.Commun.* **2014**, *312*, 62–67.

[5] Tanaami, T.; Otsuki, S.; Tomosada, N.; Kosugi, Y.; Shimizu, M.; Ishida, H. High-speed 1-frame/ms scanning confocal microscope with a microlens and Nipkow disks. *Appl. Opt.* **2002**, *41*, 4704–4708.

[6] Conchello, J. A.; Lichtman, J. W. Optical sectioning microscopy. *Nat. Methods* **2005**, *2*, 920–931.

[7] Gligorijevic, B.; Purdy, K.; Elliott, D. A.; Cooper, R. A.; Roepe, P. D. Stage independent chloroquine resistance and chloroquine toxicity revealed via spinning disk confocal microscopy. *Mol. Biochem. Parasitol.* **2008**, *159*, 7–23.

[8] Gligorijevic, B.; Bennett, T.; McAllister, R.; Urbach, J. S.; Roepe, P. D. Spinning disk confocal microscopy of live, intraerythrocytic malarial parasites. 2. Altered vacuolar volume regulation in drug resistant malaria. *Biochemistry* **2006**, *45*, 12411–12423.

[9] Egeblad, M.; Ewald, A. J.; Askautrud, H. A.; Truitt, M. L.; Welm, B. E.; Bainbridge, E.; Peeters, G.; Krummel, M. F.; Werb, Z. Visualizing stromal cell dynamics in different tumor microenvironments by spinning disk confocal microscopy. *Dis. Models & Mech.* **2008**, *1*, 155–167.

[10] Sisan, D. R.; Arevalo, R.; Graves, C.; McAllister, R.; Urbach, J. S. Spatially resolved fluorescence correlation spectroscopy using a spinning disk confocal microscope. *Biophys. J.* **2006**, *91*, 4241–4252.

[11] Cox, G.; Sheppard, C. J. Practical limits of resolution in confocal and non-linear microscopy. *Microsc. Res. Techniq.* **2004**, *63*, 18–22.

[12] Martínez-Corral, M.; Andres, P.; Ojeda-Castaneda, J.; Saavedra, G. Tunable axial superresolution by annular binary filters. Application to confocal microscopy. *Opt. Commun.* **1995**, *119*, 491–498.

[13] Nagorni, M.; Hell, S. W. 4Pi-confocal microscopy provides three-dimensional images of the microtubule network with 100- to 150-nm resolution. *J. Struct. Biol.* **1998**, *123*, 236–247.

[14] Huang, B.; Bates, M.; Zhuang, X. W. Super resolution fluorescence microscopy. *Annu. Rev. Biochem.* **2009**, *78*, 993.

[15] Schermelleh, L.; Heintzmann, R.; Leonhardt, H. A guide to super-resolution fluorescence microscopy. *J. Cell Biol.* **2010**, *190*, 165–175.

[16] Hell, S. W. Far-field optical nanoscopy. *Science* **2007**, *316*, 1153–1158.

[17] Hell, S. W. Toward fluorescence nanoscopy. *Nat. Biotechnol.* **2003**, *21*, 1347–1355.

[18] Baddeley, D.; Cannell, M. B.; Soeller, C. Three-dimensional sub-100 nm super-resolution imaging of biological samples using a phase ramp in the objective pupil. *Nano Res.* **2011**, *4*, 589–598.

[19] Hell, S. W.; Wichmann, J. Breaking the diffraction resolution limit by stimulated emission: Stimulated-emission-depletion fluorescence microscopy. *Opt. Lett.* **1994**, *19*, 780–782.

[20] Klar, T. A.; Jakobs, S.; Dyba, M.; Egner, A.; Hell, S. W. Fluorescence microscopy with diffraction resolution barrier broken by stimulated emission. *Proc. Natl. Acad. Sci. USA* **2000**, *97*, 8206–8210.

[21] Gustafsson, M. G. Nonlinear structured-illumination microscopy: Wide-field fluorescence imaging with theoretically unlimited resolution. *Proc. Natl. Acad. Sci. USA* **2005**, *102*, 13081–13086.

[22] Rego, E. H.; Shao, L.; Macklin, J. J.; Winoto, L.; Johansson, G. A.; Kamps-Hughes, N.; Davidson, M. W.; Gustafsson, M. G. Nonlinear structured-illumination microscopy with a photoswitchable protein reveals cellular structures at 50-nm resolution. *Proc. Natl. Acad. Sci. USA* **2012**, *109*, E135–E143.

[23] Shroff, H.; Galbraith, C. G.; Galbraith, J. A.; Betzig, E. Live-cell photoactivated localization microscopy of nanoscale adhesion dynamics. *Nat. Methods* **2008**, *5*, 417–423.

[24] Manley, S.; Gillette, J. M.; Patterson, G. H.; Shroff, H.; Hess, H. F.; Betzig, E.; Lippincott-Schwartz, J. High-density mapping of single-molecule trajectories with photoactivated localization microscopy. *Nat. Methods* **2008**, *5*, 155–157.

[25] Rust, M. J.; Bates, M.; Zhuang, X. Sub-diffraction-limit imaging by stochastic optical reconstruction microscopy (STORM). *Nat. Methods* **2006**, *3*, 793–796.

[26] Huang, B.; Wang, W.; Bates, M.; Zhuang, X. Three-dimensional super-resolution imaging by stochastic optical reconstruction microscopy. *Science* **2008**, *319*, 810–813.

[27] Burnette, D. T.; Sengupta, P.; Dai, Y.; Lippincott-Schwartz, J.; Kachar, B. Bleaching/blinking assisted localization microscopy for superresolution imaging using standard fluorescent molecules. *Proc. Natl. Acad. Sci. USA* **2011**, *108*, 21081–21086.

[28] Dertinger, T.; Colyer, R.; Iyer, G.; Weiss, S.; Enderlein, J. Fast, background-free, 3D super-resolution optical fluctuation imaging (SOFI). *Proc. Natl. Acad. Sci. USA* **2009**, *106*, 22287–22292.

[29] Dertinger, T.; Colyer, R.; Vogel, R.; Enderlein, J.; Weiss, S. Achieving increased resolution and more pixels with superresolution optical fluctuation imaging (SOFI). *Opt. Express* **2010**, *18*, 18875–18885.

[30] Pavani, S. R. P.; Thompson, M. A.; Biteen, J. S.; Lord, S. J.; Liu, N.; Twieg, R. J.; Piestun, R.; Moerner, W. Three-dimensional, single-molecule fluorescence imaging beyond the diffraction limit by using a double-helix point spread function. *Proc. Natl. Acad. Sci. USA* **2009**, *106*, 2995–2999.

[31] Yuen, H. P. Two-photon coherent states of the radiation field. *Phys.Rev. A* **1976**, *13*, 2226.

[32] Geissbuehler, S.; Bocchio, N. L.; Dellagiacoma, C.; Berclaz, C.; Leutenegger, M.; Lasser, T. Mapping molecular statistics with balanced super-resolution optical fluctuation imaging (bSOFI). *Opt. Nanosc.* **2012**, *1*, 1–7.

[33] Leutwyler, W. K.; Bürgi, S. L.; Burgl, H. Semiconductor clusters, nanocrystals, and quantum dots. *Science* **1996**, *271*, 933–937.

[34] Xie, R. G.; Chen, K.; Chen, X. Y.; Peng, X. G. InAs/InP/ZnSe core/shell/shell quantum dots as near-infrared emitters: Bright, narrow-band, non-cadmium containing, and biocompatible. *Nano Res.* **2008**, *1*, 457−464.

[35] Dertinger, T.; Heilemann, M.; Vogel, R.; Sauer, M.; Weiss, S. Superresolution optical fluctuation imaging with organic dyes. *Angew. Chem.* **2010**, *122*, 9631−9633.

[36] Chang, H.; Zhang, M. S.; Ji, W.; Chen, J. J.; Zhang, Y. D.; Liu, B.; Lu, J. Z.; Zhang, J. L.; Xu, P. Y.; Xu, T. A unique series of reversibly switchable fluorescent proteins with beneficial properties for various applications. *Proc. Natl. Acad. Sci. USA* **2012**, *109*, 4455−4460.

[37] Habuchi, S.; Ando, R.; Dedecker, P.; Verheijen, W.; Mizuno, H.; Miyawaki, A.; Hofkens, J. Reversible single-molecule photoswitching in the GFP-like fluorescent protein Dronpa. *Proc. Natl. Acad. Sci. USA* **2005**, *102*, 9511−9516.

[38] Zhang, X.; Chen, X.; Zeng, Z.; Zhang, M.; Sun, Y.; Xi, P.; Peng, J.; Xu, P. Development of a reversibly switchable fluorescent protein for super-resolution optical fluctuation imaging (SOFI). *ACS Nano* **2015**, *9*, 2659–2667.

[39] Michalet, X.; Pinaud, F. F.; Bentolila, L. A.; Tsay, J. M.; Doose, S.; Li, J. J.; Sundaresan, G.; Wu, A. M.; Gambhir, S. S.; Weiss, S. Quantum dots for live cells, *in vivo* imaging, and diagnostics. *Science* **2005**, *307*, 538−544.

[40] Kairdolf, B. A.; Smith, A. M.; Stokes, T. H.; Wang, M. D.; Young, A. N.; Nie, S. Semiconductor quantum dots for bioimaging and biodiagnostic applications. *Annu. Rev. Anal. Chem.* **2013**, *6*, 143−162.

[41] Xu, J.; Chang, J.;Yan, Q.; Dertinger, T.; Bruchez, M. P.; Weiss, S. Labeling cytosolic targets in live cells with blinking probes. *J. Phys. Chem. Lett.* **2013**, *4*, 2138−2146.

[42] Guizar-Sicairos, M.; Thurman, S. T.; Fienup, J. R. Efficient subpixel image registration algorithms. *Opt. Lett.* **2008**, *33*, 156−158.

[43] Geissbuehler, S.; Dellagiacoma, C.; Lasser, T. Comparison between SOFI and STORM. *Biomed. Opt. Express* **2011**, *2*, 408−420.

[44] Henriques, R.; Lelek, M.; Fornasiero, E. F.; Valtorta, F.; Zimmer, C.; Mhlanga, M. M. QuickPALM: 3D real-time photoactivation nanoscopy image processing in ImageJ. *Nat. Methods* **2010**, *7*, 339−340.

[45] Maglione, M.; Sigrist, S. J. Seeing the forest tree by tree: Super-resolution light microscopy meets the neurosciences. *Nat. Neurosci.* **2013**, *16*, 790−797.

[46] Dertinger, T.; Xu, J.; Naini, O. F.; Vogel, R.; Weiss, S. SOFI-based 3D superresolution sectioning with a widefield microscope. *Opt. Nanosc.* **2012**, *1*, 1−5.

[47] *Handbook of biological confocal microscopy*; Pawley, J. B., Ed.; Springer: New York, 2010.

[48] Ding, Y. C.; Xi, P.; Ren, Q. S. Hacking the optical diffraction limit: Review on recent developments of fluorescence nanoscopy. *Chin. Sci. Bull.* **2011**, *56*, 1857−1876.

[49] Dedecker, P.; Mo, G. C.; Dertinger, T.; Zhang, J. Widely accessible method for superresolution fluorescence imaging of living systems. *Proc. Natl. Acad. Sci. USA* **2012**, *109*, 10909−10914.

[50] Watanabe, T. M.; Fukui, S.; Jin, T.; Fujii, F.; Yanagida, T. Real-time nanoscopy by using blinking enhanced quantum dots. *Biophys. J.* **2010**, *99*, L50−L52.

[51] Zeng, Z. P.; Chen, X. Z.; Wang, H. N.; Huang, N.; Shan, C. Y.; Zhang, H.; Teng, J. L.; Xi, P. Fast super-resolution imaging with ultra-high labeling density achieved by joint tagging super-resolution optical fluctuation imaging. *Sci. Rep.* **2015**, *5*, 8359.

[52] Zhu, L.; Zhang, W.; Elnatan, D.; Huang, B. Faster STORM using compressed sensing. *Nat. Methods* **2012**, *9*, 721−723.

[53] Das, S. K.; Liu, Y.; Yeom, S.; Kim, D. Y.; Richards, C. I. Single-particle fluorescence intensity fluctuations of carbon nanodots. *Nano Lett.* **2014**, *14*, 620−625.

[54] Liu, Q.; Guo, B. D.; Rao, Z. Y.; Zhang, B. H.; Gong, J. R. Strong two-photon-induced fluorescence from photostable, biocompatible nitrogen-doped graphene quantum dots for cellular and deep-tissue imaging. *Nano Lett.* **2013**, *13*, 2436−2441.

[55] Bradac, C.; Gaebel, T.; Naidoo, N.; Sellars, M.; Twamley, J.; Brown, L.; Barnard, A.; Plakhotnik, T.; Zvyagin, A.; Rabeau, J. Observation and control of blinking nitrogen-vacancy centres in discrete nanodiamonds. *Nat.Nanotechnol.* **2010**, *5*, 345−349.